Heliyon 10 (2024) e39421

Contents lists available at ScienceDirect

Heliyon

journal homepage: www.cell.com/heliyon

Research article

Synthesis, characterization, and evaluation of pyrimidinone-linked thiazoles: DFT analysis, molecular docking, corrosion inhibition, and bioactivity studies

K.D. Venu prasad [a], Balakrishna Kallauraya [a,**], Ramesh S. Bhat [b,*], Subrahmanya I. Bhat [b,***], Vinuta Kamat [c], Mahesh Akki [c], Amit Kumar [c], K. Jyothi [d], B.R. Bharat [e]

[a] Department of Studies in Chemistry. Mangalore University, Mangalagangotri, 574 199, Karnataka, India
[b] Department of Chemistry, NMAM Institute of Technology, NITTE (Deemed to be University), Nitte, 574110, India
[c] Centre for Nano and Material Sciences, Jain (Deemed-to-be University), Jain Global Campus, Kanakapura, Bangalore, Karnataka, 562112, India
[d] Department of Chemistry, St. Joseph Engineering College, Mangalore, 575028, India
[e] Jai Research Foundation, Valvada, Vapi, Gujarat, 396105, India

ARTICLE INFO

Keywords:
Pyrimidinone
Biginelli reaction
Thiazole
Antibacterial
Corrosion inhibition
Hantzsch synthesis

ABSTRACT

The paper describes the construction of a new series of pyrimidinone-linked thiazole derivatives through bromination of the initial Biginelli reaction product followed by the Hantzsch thiazole synthesis route. Various analytical techniques, including FT-IR, ^{1}H NMR, ^{13}C NMR, and LCMS analysis, were employed to confirm the formation of the products. The synthesized compounds were primarily evaluated for their antibacterial activity, with a specific focus on their IC_{50} values. Compound **4c** demonstrated the most potent efficacy, displaying MIC and MBC values that varied from 0.23 to 0.71 mg/mL and 0.46–0.95 mg/mL, respectively. The anti-inflammatory potential was also observed in analogs **4a** and **4c** with marked activity in the 33.2–82.9 μM concentration range. Moreover, compounds **4a**, and **4c** demonstrated strong antioxidant effects, as reflected by their excellent IC_{50} values of **38.6**–**43.5** μM respectively. DFT investigation showed that *B. cereus* was more susceptible, and *E. coli* was more resistant, with chloro-substituted compounds exhibiting potential reactivity. Some molecules with chloro-substituents showed promising results in density functional theory when compared to other substituents. In addition, the molecules underwent a corrosion study and demonstrated a high level of inhibition efficiency (**4c**) in comparison to other molecules. Further *in silico* studies of the synthesized thiazoles confirmed the good interactions with the target.

1. Introduction

The importance of modified heterocyclics and heterocyclic rings in the treatment of a range of chronic illnesses is well-acknowledged [1,2]. Dealing with infectious infections caused by bacteria and fungi is quite a challenging task, given the rise in multi-drug-resistant microbial pathogens. For medicinal chemists, one of the most difficult problems is to produce novel molecules

* Corresponding author.
** Corresponding author.
*** Corresponding author.
E-mail addresses: bkallauraya@gmail.com (B. Kallauraya), rameshbhat@nitte.edu.in (R.S. Bhat), subrahmanya@nitte.edu.in (S.I. Bhat).

https://doi.org/10.1016/j.heliyon.2024.e39421
Received 6 August 2024; Received in revised form 14 October 2024; Accepted 14 October 2024
Available online 18 October 2024

with an active nucleus to battle germs that are resistant to drugs. Heterocycles are crucial building blocks for the suppression of numerous deadly infections [3,4]. Due to its potential as a medicinal agent, incorporating five-membered heterocycles is always an exciting task for chemists.

Among the five-membered heterocyclic compounds, thiazoles are known to exhibit a wide range of biological actions, including anticancer [5], antidiabetic [6–8], antimicrobial [9,10] tubercular [11], antioxidant [12], anti-inflammatory [13–15] activities. In addition, the building blocks of several natural compounds such as vitamin B1 (thiamine) include thiazole and thiazolone moieties. Numerous physiologically active medications, including meloxicam (anti-inflammatory), abafungin (antifungal), tiazofurin (anti--neoplastic), and sulfathiazole (anti-microbial), also include them. Pharmacological research indicates that the incorporation of the thiazole nucleus boosts the biological activity of various compounds [16–21].

Density Functional Theory (DFT) has indeed transformed the landscape of computational chemistry and solid-state physics, allowing researchers to tackle larger and more complex systems than would be feasible with traditional wave function methods. Its strength lies in balancing computational efficiency with reasonably accurate predictions of electronic structures, making it a go-to tool for many applications. Despite its widespread use, DFT has notable limitations, particularly in the treatment of non-local interactions like dispersion forces. This has become a significant concern as researchers explore larger molecular systems where such interactions become more relevant [22,23]. The various approximations within DFT can lead to discrepancies in energy and structural predictions, highlighting the need for ongoing validation and refinement of these methods. Additionally, the adaptability of DFT for performing numerous calculations efficiently allows for studies of dynamic processes, such as time evolution of systems, which can be particularly valuable in fields like materials science and biochemistry. The continuous development of new functionals and hybrid methods seeks to address some of these shortcomings, but challenges remain. Research into improving DFT's ability to accurately describe dispersion and other weak interactions is an active area, as is the quest for functionals that can better capture the nuances of electronic correlation in larger systems [24,25].

On the other hand, dihydropyrimidinones are important heterocyclic compounds discovered by Pietro Biginelli through a three-component reaction, first reported in 1893 [26]. These densely functionalized Biginelli compounds are known for their potent biological activities such as calcium channel blockade, anti-inflammatory, antioxidant, antifungal, antifilarial. Antihypertensive, analgesic, anticancer and antimicrobial functions [27–29]. Additionally, significant enhancement in pharmacological activities has been reported when these dihydropyrimidinones were linked with other heterocycles [27,30–32]. Thus, the hybrid compounds containing dihydropyrimidinones and thiazoles may have substantial therapeutical potential. Furthermore, pyrimidinone linked thiazole scaffolds with derivatization at 2-amino position of thiazole core has not yet explored.

Herein we report the synthesis of new thiazole coupled 6-methyl-3,4-dihydropyrimidin-2(1*H*)-one hybrid scaffold through the Hantzsch reaction of substituted thiourea with 2-bromomethylketones of dihydropyrimidinones which were derived using well-known Biginelli three-component reaction. Interestingly, the designed products can be further derivatized at the 2-amino position of the thiazole moiety and 4-position of pyrimidinone core to get diversified hybrid molecules. All the final compounds were confirmed using FT IR, ^{1}H NMR, ^{13}C NMR, and LC-MS data. Further, the final hybrid molecules were evaluated for their antibacterial, antioxidant, and *in-vitro* anti-inflammatory activity and studied for their corrosion inhibition efficiency.

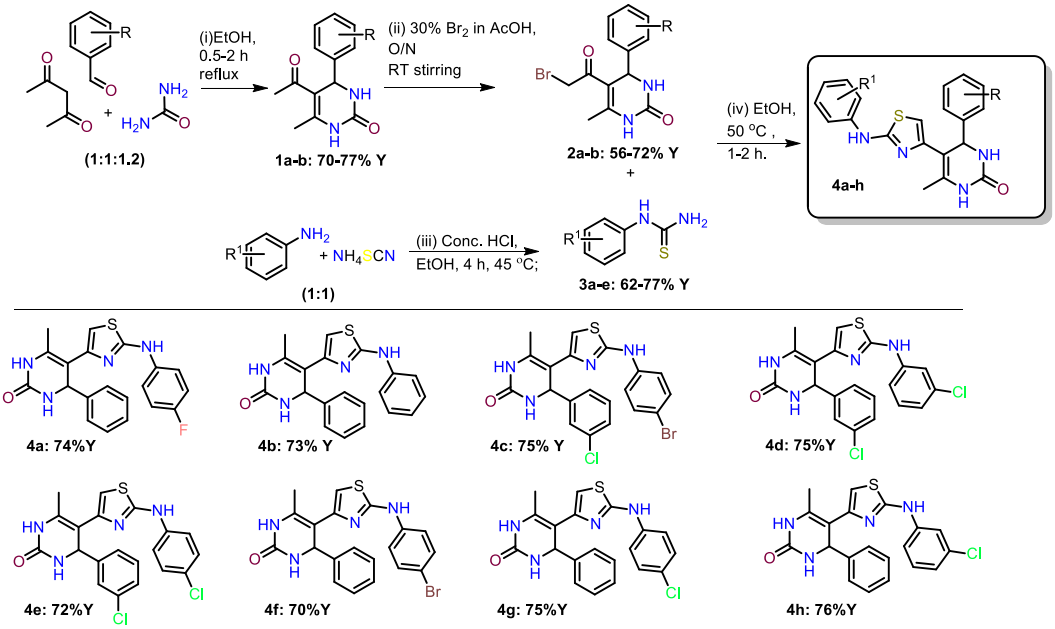

Scheme 1. Synthesis of (4-substituted phenyl)-5-(2-([substituted phenyl] amino) thiazol-5-yl)-6-methyl-3,4-dihydropyrimidin-2(1*H*)-one (**4a-h**).

2. Results and discussion

2.1. Chemistry

The synthetic pathways and structures of the final thiazole-dihydropyrimidinone hybrid compounds (**4a-h)** are shown in Scheme 1. Initially, dihydropyrimidinones (**1a-c)** were synthesized through Biginelli three-component reaction of acetylacetone (1 equiv.) and urea or thiourea (1.2 equiv.) with aldehydes (1 equiv.) in presence of aqueous HCl catalyst in ethanol solvent under reflux. Then obtained dihydropyrimidinones were subjected to bromination in acetic acid to obtain 5-(2-bromoacetyl)-6-methyl-4-phenyl-3,4-dihydropyrimidin-2(1*H*)-one derivative (**2a-c**). On the other hand, substituted thiourea (**3a-e**) was obtained through a 1:1 reaction of aniline derivatives with ammonium thiocyanate in the presence of ethanolic HCl media. Finally, 5-(2-bromoacetyl)-6-methyl-4-phenyl-3,4-dihydropyrimidin-2(1*H*)-one derivative and aromatic substituted thiourea were reacted in absolute ethanol at 50 °C to yield thiazole linked dihydropyrimidinone hybrid molecules **4a-h**. Furthermore, the synthesized compounds were purified through recrystallization with methanol. Thin-layer chromatography (TLC) was used to assess the purity of the compounds. The structure of all the products was confirmed using various spectroscopic techniques including ^{1}H NMR, ^{13}C NMR, LCMS, FTIR, and mass. It was found that the synthesized compounds demonstrated excellent agreement with the expected spectral data (For characterization data refer Table 1).

Reaction conditions: (i) EtOH, 0.5–2 h reflux; (ii) 30 % Br_2 in AcOH, O/N RT stirring; (iii) Conc. HCl, EtOH, 4 h, 45 °C; (iv) EtOH, 50 °C, 1–2 h.

2.2. Biological analysis

2.2.1. Antibacterial studies

The effectiveness of synthetic compounds in fighting bacteria was evaluated using the micro-dilution method. A panel of six bacteria was tested, and the minimal inhibitory concentration (MIC) and minimal bactericidal concentration (MBC) were used as measures of their activity. The compounds being studied demonstrated a satisfactory level of antibacterial activity, as indicated in Table 2. The MIC values ranged from 0.17 to >3.74 mg/mL, while the MBC values ranged from 0.23 to >3.75 mg/mL. The highest level of activity was observed for compound **4c**, with concentrations ranging from 0.23 to 0.71 mg/mL and 0.46–0.95 mg/mL. *E. coli* proved to be the most resilient bacterium, while *B. cereus* appeared to be the least resistant. By assessing the MIC and MBC against a panel of six bacteria, the antibacterial activity of the synthesized compounds was assessed using the micro-dilution method. Table 2 shows that the compounds had moderate to good antibacterial activity, with MBC values ranging from 0.23 to >3.75 mg/mL and MIC values ranging from 0.17 to >3.74 mg/mL. A MIC of 0.23–0.71 mg/mL and an MBC of 0.46–0.95 mg/mL, respectively, indicated that compound **4c** had the highest activity. According to the results, *E. coli* had the highest resilience, whereas *B. cereus* was the most sensitive bacterium. At MIC/MBC values of 0.18/0.24 mg/mL, compound **4d** showed the highest activity against *E. coli*, while compound **4h** indicated considerable activity against both *B. cereus* and *S. typhimurium*.

MIC and MBC values of 0.23/0.47 mg/mL were demonstrated for compounds **4a** and **4h** against *E. cloacae*, while compounds **4c** and **4e** also demonstrated good activity against *E. coli*. When it came to *S. typhimurium*, compound **4a** also showed promising results. Overall, the antibacterial activity of these compounds was modest to moderate. Three of the most active compounds (**4b**, **4c**, and **4d**) were evaluated against *P. aeruginosa*, *E. coli*, and methicillin-resistant *Staphylococcus aureus* (MRSA). Comparing all three products against ampicillin and streptomycin, which lacked bactericidal activity, it was found that the former two were less successful against MRSA. Compound **4d** seemed to be more effective than ampicillin against the *P. aeruginosa* strain, but ultimately, no compound outperformed the reference drug in terms of effectiveness against *E. coli* (Table 3). Another evaluation of the compounds was that they inhibited the production of biofilms. Regretfully, no chemical showed any noteworthy efficacy in this aspect.

2.2.2. In vitro anti-inflammatory activity (denaturation of bovine serum albumin method)

The inhibitory effects on the denaturation of the proteins can be assessed using a heat-induced protein denaturation procedure, with diclofenac sodium serving as the standard drug. It was confirmed that thiazole analogs had anti-inflammatory properties in vitro. The results are shown in Table 4 and include the percentage inhibition of the thiazole analogs as well as the IC50 values of the drugs. The results are shown in Fig. 1. It was evident from the data that 4a and 4c, two thiazole analogs, had superior activity.

Table 1
Characterization data of (4-substituted phenyl)-5-(2-([substituted phenyl] amino) thiazol-5-yl)-6-methyl-3,4-dihydropyrimidin-2(1*H*)-one.

Compounds	R	R^1	%Yield (mp °C)	Color and crystal Form	Molecular formula (Mol. Weight)	% S Found (Calculated)
4a	H	*p*-F	74 (141)	Orange needles	$C_{20}H_{17}FN_4OS$ (380.11)	8.38 (8.43)
4b	H	H	73 (136)	Pale white	$C_{20}H_{18}N_4OS$ (362.45)	8.80 (8.85)
4c	*m*-Cl	*p*-Br	75 (165)	Pale yellow	$C_{20}H_{16}BrClN_4OS$ (475.79)	6.71 (6.74)
4d	*m*-Cl	*m*-Cl	75 (164)	Yellow crystals	$C_{20}H_{16}$ Cl_2N_4OS (431.34)	7.40 (7.43)
4e	*m*-Cl	*p*-Cl	72 (166)	Pale yellow	$C_{20}H_{16}$ Cl_2N_4OS (431.34)	7.40 (7.43)
4f	H	*p*-Br	70 (170)	Pale Brown crystals	$C_{20}H_{17}BrN_4OS$ (441.34)	7.23 (7.27)
4g	H	*p*-Cl	75 (169)	Yellow crystals	$C_{20}H_{17}ClN_4OS$ (396.89)	8.04 (8.08)
4h	H	*m*-Cl	76 (170)	Yellow crystals	$C_{20}H_{17}ClN_4OS$ (396.89)	8.04 (8.08)

Table 2
Antibacterial activity of synthesized compounds **4a-h**.

Compounds		*S. aureus*	B. cereus	L. monocytogenes	*E. coli*	*S. typhimurium*	*E. cloacae*
4a	**MIC**	0.68 ± 0.17	0.33 ± 0.07	0.33 ± 0.07	>3.76	>3.76	0.21 ± 0.01
	MBC	0.92 ± 0.01	0.45 ± 0.02	0.45 ± 0.01	>3.77	>3.76	0.47 ± 0.01
4b	**MIC**	0.92 ± 0.02	0.47 ± 0.03	0.72 ± 0.18	0.36 ± 0.07	0.36 ± 0.07	0.36 ± 0.07
	MBC	1.88 ± 0.01	0.94 ± 0.01	0.94 ± 0.02	0.46 ± 0.01	0.47 ± 0.01	0.47 ± 0.01
4c	**MIC**	0.72 ± 0.21	0.25 ± 0.01	0.72 ± 0.18	0.25 ± 0.02	0.25 ± 0.01	0.72 ± 0.20
	MBC	0.96 ± 0.03	0.48 ± 0.02	0.95 ± 0.01	0.48 ± 0.01	0.48 ± 0.02	0.95 ± 0.00
4d	**MIC**	1.43 ± 0.41	0.72 ± 0.19	0.72 ± 0.19	0.18 ± 0.01	0.72 ± 0.20	0.72 ± 0.20
	MBC	1.90 ± 0.01	0.96 ± 0.02	0.96 ± 0.02	0.25 ± 0.02	0.96 ± 0.00	0.96 ± 0.01
4e	**MIC**	1.42 ± 0.41	0.72 ± 0.19	0.72 ± 0.17	0.24 ± 0.01	0.47 ± 0.01	0.72 ± 0.18
	MBC	1.90 ± 0.02	0.96 ± 0.01	0.96 ± 0.02	0.47 ± 0.01	0.94 ± 0.02	0.95 ± 0.01
4f	**MIC**	2.30 ± 0.78	1.42 ± 0.39	0.71 ± 0.18	>3.74	0.71 ± 0.18	0.71 ± 0.18
	MBC	3.76 ± 0.02	1.89 ± 0.00	0.95 ± 0.02	>3.76	0.95 ± 0.02	0.95 ± 0.01
4g	**MIC**	1.42 ± 0.00	0.71 ± 0.21	0.71 ± 0.21	0.36 ± 0.10	0.71 ± 0.20	0.71 ± 0.20
	MBC	1.89 ± 0.01	0.95 ± 0.03	0.95 ± 0.02	0.48 ± 0.01	0.95 ± 0.00	0.95 ± 0.01
4h	**MIC**	1.42 ± 0.39	0.46 ± 0.01	0.36 ± 0.12	>3.76	0.36 ± 0.10	0.24 ± 0.01
	MBC	1.89 ± 0.02	0.95 ± 0.02	0.48 ± 0.01	>3.76	0.48 ± 0.01	0.48 ± 0.01
Streptomycin	**MIC**	0.11 ± 0.03	0.03 ± 0.02	0.16 ± 0.01	0.11 ± 0.02	0.11 ± 0.00	0.03 ± 0.01
	MBC	0.21 ± 0.02	0.06 ± 0.01	0.31 ± 0.00	0.21 ± 0.01	0.21 ± 0.02	0.06 ± 0.02
Ampicillin	**MIC**	0.11 ± 0.01	0.11 ± 0.01	0.16 ± 0.01	0.16 ± 0.01	0.11 ± 0.01	0.11 ± 0.01
	MBC	0.16 ± 0.02	0.16 ± 0.01	0.31 ± 0.03	0.21 ± 0.02	0.21 ± 0.00	0.16 ± 0.01

Table 3
Antibacterial and inhibition activity.

Compounds		MRSA	*P. aeruginosa*	*E. coli*	MIC	0 % MIC
4b	MIC	0.93 ± 0.00	0.24 ± 0.00	0.93 ± 0.00	14.58	7.07
	MBC	1.87 ± 0.00	0.46 ± 0.00	1.87 ± 0.00		
4c	MIC	0.46 ± 0.00	0.22 ± 0.00	0.46 ± 0.00	19.96	8.83
	MBC	0.93 ± 0.00	0.46 ± 0.00	0.93 ± 0.00		
4d	**MIC**	**0.95 ± 0.00**	**0.24 ± 0.00**	**0.95 ± 0.00**	**4.32**	**NE**
	MBC	1.87 ± 0.00	0.46 ± 0.00	1.87 ± 0.00		
Streptomycin	MIC	0.09 ± 0.00	0.04 ± 0.00	0.09 ± 0.00	71.93	55.41
	MBC	/	0.09 ± 0.00	0.19 ± 0.00		
Ampicillin	MIC	/	0.19 ± 0.01	0.19 ± 0.00	67.35	30.34
	MBC	/	/	/		

The IC_{50} values of the thiazole pyrimidine analogs were in the range, of 33.2–82.9 μM. The anti-inflammatory profiles of the samples varied with the substituents and their positions. Among the synthesized compounds fluoro derivatives showed excellent inhibition. Compounds **4a** and **4c** show excellent inhibition than the normal drug diclofenac sodium.

2.2.3. Antioxidant assay by DPPH method

The DPPH method assessed the thiazole analog's ability to scavenge radicals. The compounds displayed varying antioxidant capabilities when compared to conventional ascorbic acid.

Table 5 tabulates the findings of the DPPH scavenging. With IC50 values of 43.5 μM and 38.6 μM, respectively, compounds 4a and 4c demonstrated the greatest antioxidant ability. In Fig. 2, the data is displayed as a bar graph. Among the thiazoles, fluoro signifies excellent inhibition than the standard drug.

Std: Ascorbic acid.

Table 4
Anti-inflammatory analysis in terms of IC_{50} values of the prepared compounds.

Compounds- **4**	IC_{50} (μM)
4a	**33.2**
4b	44.2
4c	**34.0**
4d	40.6
4e	51.3
4f	63.8
4g	36.9
4h	82.9
Std	34.8

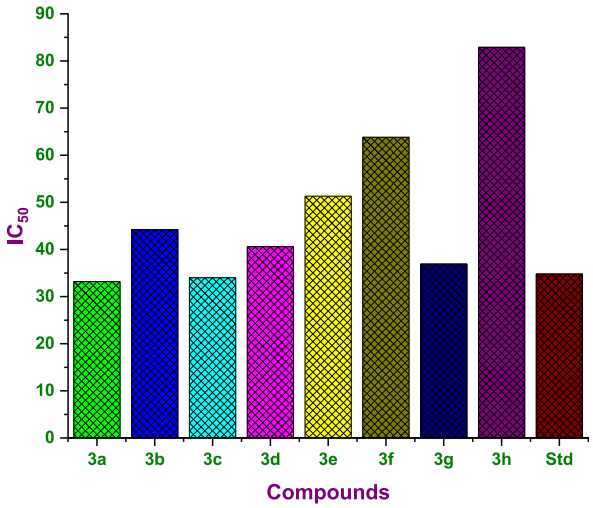

Fig. 1. Graphical picture of the anti-inflammatory actions.

Table 5
DPPH radical scavenging capacity as measured by the target thiazoles' IC50 values (4a–h).

compounds	IC_{50} (μM)
4a	**38.6**
4b	52.1
4c	**43.5**
4d	67.8
4e	55.7
4f	49.9
4g	73.5
4h	62.6
Std	45.6

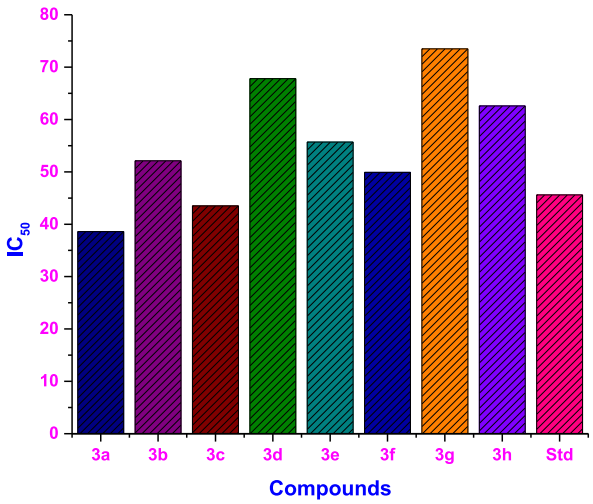

Fig. 2. Visual depictions of the antioxidant activities.

2.2.3.1. Molecular docking studies. To determine the potential binding mode of the active compounds against the target protein COX-2, docking studies were conducted. The molecular docking analysis showed promising binding energies for all the compounds, which ranged from −10.3 to −9.3 kcal/mol, as detailed in Table 6. Compound **4a** establishes one hydrogen bonding interaction at the protein's active site (Fig. 3). The hydrogen bonding was raised from the amine group of the pyrimidine ring with CYS26 amino acid

residue. Additionally, compound **4a** engages carbon-hydrogen bond with CYS22 and VAL141 residue, pi-doner hydrogen bond with CYS32, pi sulfur with CYS145, amide pi-stacked with CYS21 residue and pi-alkyl interaction with ARG29, PRO139 and ALA142 amino acid residues.

Similarly compound **4d** forms two hydrogen bonding interactions at the active site of the protein (Fig. 4). The first hydrogen bonding interaction was raised from the amine group of the pyrimidine ring with ASN361 amino acid residue. The second hydrogen bonding interaction was raised from a sulfur atom of thiazole ring with ARG362 amino acid residue. Additionally, it engages in carbon-hydrogen bonds with SER129 residue, pi-pi stacked interaction with PHE128 residue, and alkyl interactions with LEU13, TRP125, and PHE128 amino acid residues.

These interactions highlight the potential binding modes and affinities of the compounds, suggesting their capability to effectively engage with the target protein. The detailed insights into hydrogen bonding and other non-covalent interactions provide a comprehensive understanding of the binding mechanisms, paving the way for further optimization and development of these compounds as potential therapeutic agents.

2.3. Corrosion analysis

2.3.1. Potentiodynamic polarization (PP) study

The test results of the newly synthesized compound showed a notable inhibition effect on the MS substrate, resembling the work of a biophysicist. The findings can be observed in Table 7. The PP plots, which demonstrated exceptional performance at room temperature, are displayed in Fig. 5. Several electrochemical parameters were measured and are shown in Table 7. These parameters include corrosion current (i_{corr}), corrosion potential (E_{corr}), cathodic slope (βc), anodic slope (βa), and inhibition efficiency (IE). When comparing the i_{corr} of MS with and without the inhibitor, it became evident that the inhibitor (**4c)** showed greater effectiveness in reducing corrosion. With the inhibitor, the MS showed a remarkable inhibition efficiency of 69.35 % and consequently exhibited superior corrosion resistance when compared to the MS without the inhibitor. The enhancement can be credited to the adsorption of the inhibitor on the MS surface. Interestingly, the corrosion rate was found to be highest in mild steel, whereas the inhibitor showed remarkable efficiency at room temperature [33].

The adsorption of the inhibitor (4c) on the compound on mild steel/solution interfaces plays a crucial role in determining corrosion behaviour. The corrosion potential of MS in comparison to the blank was shifted to a cathodic state. The PP curve (Fig. 5) shows inhibition of both the anodic and cathodic reactions and the inhibitor functions as a mixed type in this case.

2.3.2. Electrochemical impedance (EIS) analysis

Deviation from ideal semicircular Nyquist plots suggests an uneven and heterogeneous surface, adsorption of inhibitors, or the formation of a porous layer. The impedance spectrum supports the charge transfer mechanism. For effective inhibition, it is important to have larger magnitudes for capacitive and inductive loops, as demonstrated in the current experiment. Fig. 6 displays the Nyquist plots of mild steel in 1 M HCl solution at room temperature, both with and without inhibitors. When the inhibitor is not present, the mild steel exhibits a lower impedance module and a higher corrosion rate, as shown in Table 7. However, when an inhibitor is introduced, the radius of the impedance module increases, as illustrated in Fig. 6. This leads to an improvement in corrosion inhibition efficiency, as shown in Table 7. The depression in the figure illustrates the metal surface irregularities that can arise from corrosion [33]. The corrosion resistance can be observed to decrease significantly as the diameter of the capacitive loop decreases.

2.4. DFT (Density Functional Theory)

2.4.1. Frontier molecular orbital analysis

In the compounds that were examined, it was observed that interactions of the LP-LP and LP-bond pair types were more prevalent, as per the molecular orbital theory. This is due to the interaction between the HOMO and the LUMO. Table 8 presents the calculated HOMO-LUMO energies, energy gap, dipole moment, electronegativity, global hardness, and ionization energy. The structure of synthesized compound **4a** is shown in Fig. 7a and b, showing the HOME and LUMO characteristics. From the optimized geometry of the compounds, it is evident that the molecular orbital analysis reveals the dominance of p-type atomic orbitals in the Frontier molecular orbitals. A larger HOMO-LUMO gap typically leads to a less reactive electronic system compared to a smaller gap. Furthermore, the energy gap between the HOMO and the LUMO elucidates the mechanism by which charges can move through molecules. The size of

Table 6
The binding affinity of the synthesized compounds.

Code	Binding Affinity (kcal/mol)
4a	−10.3
4b	−9.3
4c	−9.4
4d	−9.9
4e	−9.7
4f	−9.4
4g	−9.4
4h	−9.7

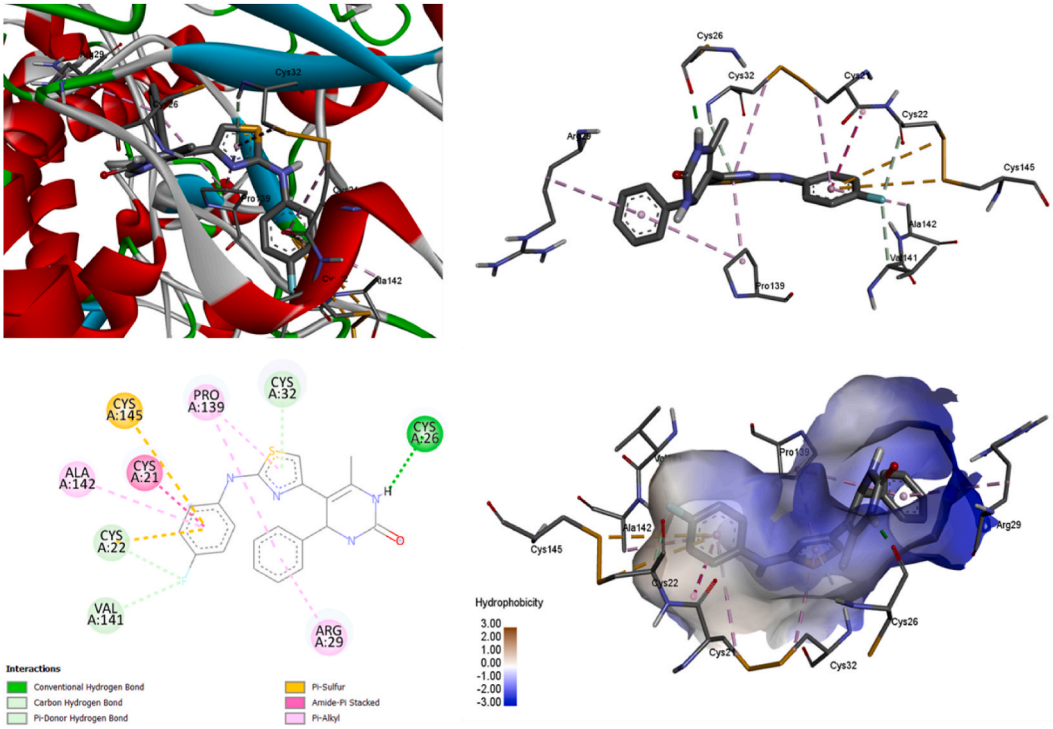

Fig. 3. The crystal structure of the COX-2 protein (PDB:3LN1) with active compound **4a.**

the HOMO-LUMO gap can indicate a reactivity of the molecules. Smaller gaps often suggest that a molecule is more reactive or prone to undergoing chemical changes, as less energy is required to promote an electron from the HOMO to the LUMO. A larger HOMO-LUMO gap can correlate with increased stability in a molecular system, as it requires more energy to promote electrons to higher energy levels. Pauling discovered the phenomenon of an electronegative atom in a compound attracting an electron towards itself. One can analyze the literature to find various characteristics such as hardness, ionization potential, electronegativity, chemical potential, electron affinity, and global softness. Fig. 8 displays the optimized structures of the synthesized compound **4a**.

Using LUMO orbital energies and HOMO orbital energies, one can represent both the electron affinity (EA) and ionization energy (IE). The hardness (η) represents the difference in orbital energies between HOMO and LUMO. The stability of the chemical system is closely associated with its hardness. Quantum chemical properties of the molecules under investigation were calculated using the B3LYP technique and the 6-31G (d,p) basis set. The results can be found in Table 8. Based on the findings presented in Tables 8 and it is evident that among the molecules being studied, **4c** exhibits the smallest energy gap of 0.2831 eV, while **4a** demonstrates the largest energy gap of 0.2874 eV. These findings indicate that **4c** exhibits a higher level of reactivity compared to the other synthesized compounds. Compounds **4c** and **4d** exhibit a soft nature and possess greater polarizability compared to other compounds in this series. This is supported by the low global hardness of compound **4c** (0.1418 eV) and the significantly negative value of its chemical potential (−0.1772 eV). Compound **4d** possesses a remarkable ability to allure withdrawing electrons, signifying its significant electronegativity (0.1772 eV), making it an electrophile [34,35].

3. Experimental

3.1. Materials, methods, and instrumentations

All the compounds utilized in the investigation were obtained from reputable suppliers such as Sigma-Aldrich or Hi-Media and used as received. A 400 MHz Bruker Avance II NMR spectrometer was used to obtain the ^{1}H and ^{13}C NMR spectra using DMSO solvent and TMS (tetramethyl silane) as an internal standard. Mass spectra were obtained using an LC-MS instrument (SHIMADZU LCMS-8030) operating at 70 eV. The chemicals were dispersed within pellets of potassium bromide, and a SHIMADZU FTIR 157 spectrophotometer was used to acquire the FT-IR spectra. Thin-layer chromatography (TLC) was employed to assess the purity of the compounds using Merck silica gel plates and an ethyl acetate: hexane (3:7) mobile phase.

3.2. General procedure for the synthesis of 5-acetyl-6-methyl-4-phenyl-3,4-dihydropyrimidin-2(1H)-ones (1a-b)

A solution of the substituted aldehydes (3 mmol), 1,3-dicarbonyl compound (3 mmol), and urea (3.6 mmol), were dissolved in

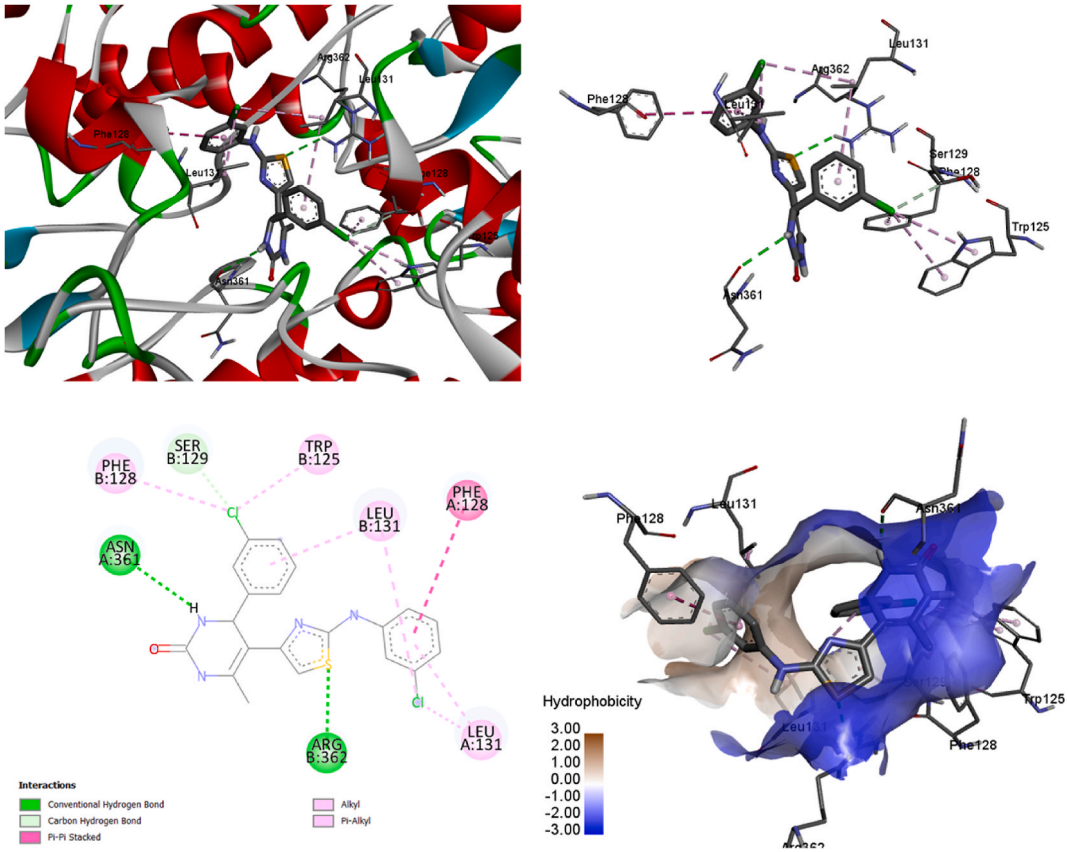

Fig. 4. The crystal structure of the COX-2 protein (PDB:3LN1) with active compound **4d.**

Table 7
PP studies on mild steel in 1 M HCl solution with and without of inhibitor (**4c**).

Compound(4c)	i_{corr} (μA/cm^2)	E_{corr} (V)	βc (mV/dec)	βa (mV/dec)	IE (%)
With inhibitor	327.00	−0.466	6.859	10.289	69.35
Without inhibitor	1067.00	−0.470	6.048	16.730	–

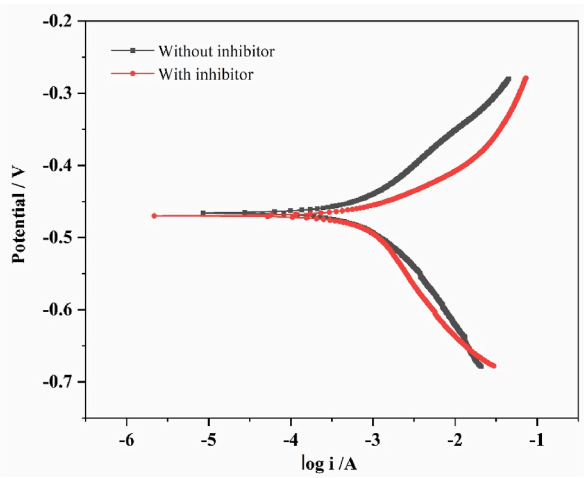

Fig. 5. PP plot of mild steel in 1 M HCl with and without inhibitor.

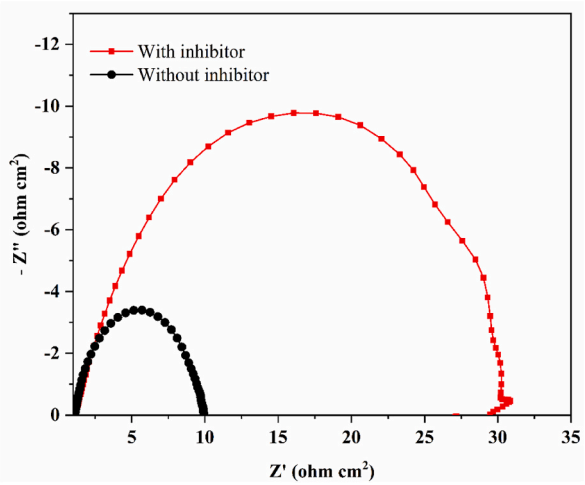

Fig. 6. Electrochemical impedance plots for mild steel in 1 M HCl with and without inhibitor(4c).

Table 8
Quantum chemical parameters for the synthesized compounds (**4a-h**).

Compounds	4a	4b	4c	4d	4e	4f	4g	4h
Parameters (conditions)	Values							
E_{HOMO}, eV	−0.3146	−0.3103	−0.3151	−0.3161	−0.3207	−0.3151	−0.3140	−0.3177
E_{LUMO}, eV	−0.0271	−0.0238	−0.0320	−0.0314	−0.0336	−0.0315	−0.0304	−0.0306
Ionization potential I, eV	0.3146	0.3103	0.3151	0.3161	0.3207	0.3151	0.3139	0.3177
Electron affinity A, eV	0.0271	0.0238	0.0320	0.0314	0.0336	0.0315	0.0304	0.0306
ΔN	1.8094	1.8098	1.8090	1.8090	1.8086	1.8091	1.8092	1.8089
ΔE, eV	0.2874	0.2865	0.2831	0.2847	0.2871	0.2836	0.2836	0.2871
Electronegativity χ, eV	0.1709	0.1670	0.1736	0.1738	0.1772	0.1733	0.1722	0.1742
Global hardness η, eV	0.1437	0.1432	0.1415	0.1424	0.1436	0.1418	0.1418	0.1436
Softness S, eV^{-1}	6.9580	6.9818	7.0651	7.0249	6.9657	7.0517	7.0537	6.9657

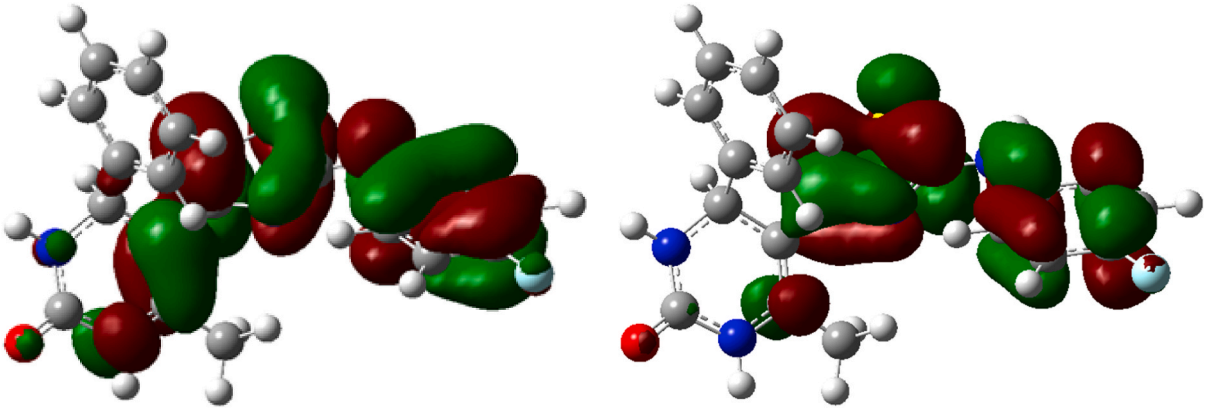

Fig. 7. (a). HOMO structure of the compounds **4a**
Fig. 7b. LUMO structure of the compound **4a**.

ethanol solvent and stirred at reflux for 0.5–2 h. Then the reaction mixture was cooled to room temperature and poured into 50 mL ice cold water. The obtained precipitate was filtered and washed with ice water followed by ethanol (95 %) and dried under vacuum. Finally, pure products (**1a-b**) were obtained through recrystallization from hot ethanol.

3.2.1. 5-Acetyl-6-methyl-4-phenyl-3,4-dihydropyrimidin-2(1H)-one (1a)

Yield: 72 %, white solid, mp. 233 °C (Lit. 235 °C [36]). IR (KBr) (υ cm^{-1}): 1725 (C=O str.), 3090 (-CH- str.), 3241 (NH str.). ^{1}H NMR (DMSO-d_6, 400 MHz) δ in ppm = 2.04 (s, 3H, CH_3), 2.26 (s, 3H, -$COCH_3$), 5.19 (d, 1H, J = 4.5 Hz, CH), 7.13 (m, 5H, Ar), 7.75 (s, 1H,

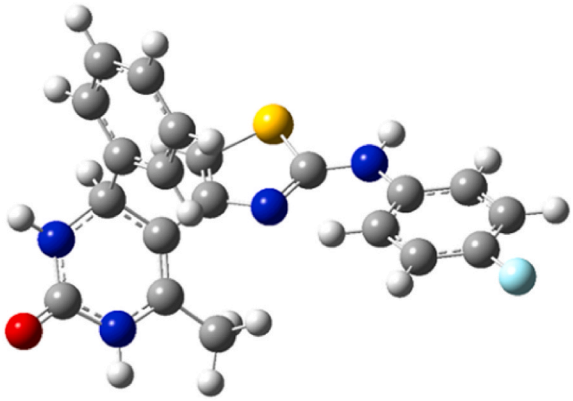

Fig. 8. Optimized structures of the compound **4a**.

NH), 9.12 (s, 1H, NH). ^{13}C NMR (100 MHz, DMSO-d_6) δ in ppm: 18.6 (-*C*H$_3$), 33.4 (*C*H$_3$CO-), 52.8 (ring *C*H), 127.0, 127.3, 127.8, 128.4, 146.1, 152.1 (ring *C*=O), 185.7 (CH$_3$-*C*=O).

3.2.2. 5-Acetyl-4-(3-chlorophenyl)-6-methyl-3,4-dihydropyrimidin-2(1H)-one (1b)

Yield: 56 %, white solid, mp. 214 °C. IR (KBr) *Cm*$^{-1}$): (υ cm^{-1}): 1717 (C=O str.), 3092 (-CH- str.), 3246 (NH str.). ^{1}H NMR (DMSO-d_6, 400 MHz) δ in ppm = 2.04 (s, 3H, CH$_3$), 2.22 (s, 3H, CH$_3$), 5.29 (d, 1H, J = 4 Hz, CH), 7.03–7.13 (m, 4H, Ar), 7.70 (s, 1H, NH), 9.0 (s, 1H, NH).

Mass (*m/z*): 264 (M$^+$), 266 (M+2).

3.3. General procedure for the synthesis of 5-(2-bromoacetyl)-6-methyl-4-phenyl-3,4-dihydropyrimidin-2(1H)-ones (2a-b)

Compound (**1a** or **1b**) (1 equvi.) and glacial acetic acid (10 mL) were taken in a 25 mL two necked RB flask connected to addition flask and stirred at RT. A solution of bromine (30 % in acetic acid) was added dropwise using addition flask with continuous stirring until the colour of the bromine persisted. The reaction mixture was then allowed to stand at room temperature overnight. The solid separated was then filtered and washed with petroleum ether and dried under vacuum. It was then recrystallized from glacial acetic acid and taken for next step.

3.4. General procedure for the synthesis of for the synthesis of aryl thioureas (3a-e)

A mixture of aniline (0.1 mol), ammonium thiocyanate (0.1 mol) and 50 mL 20 % aqueous hydrochloric acid were taken in an RB flask, heated to 45 °C and stirred continuously for 3 h. After cooling, the solid separated was collected by filtration, washed thoroughly with water, and dried under vacuum and recrystallized further from ethanol solvent.

N-Phenyl thiourea 3a: Pale yellow crystals. mp 153 °C (Lit. 154 °C [37]), Yield: 75 %.

4-Chlorophenyl thiourea 3b: Greyish-black microcrystals. mp: 146 °C, Yield: 70 %.

3-Chlorophenyl thiourea 3c: Greyish microcrystals. mp: 148 °C, Yield: 60 %.

4-Bromophenyl thiourea 3d: Brown microcrystals. mp: 147 °C, Yield: 65 %.

4-Fluorophenyl thiourea 3e: Orange microcrystals. mp: 152 °C, Yield: 70 %.

3.5. General procedure for the synthesis of (substituted-phenyl)-5-(2-([substituted phenyl] amino)-2,3-dihydrothiazol-5-yl)-6-methyl-3,4-dihydropyrimidin-2(1H)-one (4a-h)

An equimolar mixture of aryl thiourea (**3a-e)** (0.01 mol) and bromo-derivatives (**2a-b**) (0.01 mol) in absolute ethanol (25 mL) was heated to 50 °C and stirred continuously for 1–2 h. The solid that separated after the reaction mixture was cooled to room temperature was filtered, washed with water, recrystallized from ethanol, and dried under vacuum to produce the title compounds.

3.5.1. 5-(5-([4-fluorophenyl]amino)thiazol-2-yl)-6-methyl-4-phenyl-3,4-dihydropyrimidin-2(1H)-one (4a)

Yield: 2.81 g (74 %), orange needles, mp. 141 °C. IR (KBr) (υ cm^{-1}): 1600 (C=O str.), 3090 (-CH- str.), 3220 (NH str.). ^{1}H NMR (DMSO-d_6, 400 MHz) δ in ppm = 2.63 (s, 3H, -CH$_3$), 6.04 (s, 1H), 6.74 (s, 1H), 7.45 (d, 2H, J = 14.4 Hz), 7.51 (d, 2H, J = 15 Hz), 7.88-7.51 (m, 6H, Ar), 10.23 (s, 2H, -NH). ^{13}C NMR (100 MHz, DMSO-d_6) δ in ppm: 17.2 (*C*H$_3$), 39.8 (ring-*C*H), 98.9, 113.7, 125.0, 124.7, 134.0, 135.9, 144.3, 154.6 (ring *C*=O), 168.4, 170.8 (Thiazole C_2). Mass:(*m/z*): 381 (M$^+$).

3.5.2. 6-Methyl-4-phenyl-5-(5-(phenylamino)thiazol-2-yl)-3,4-dihydropyrimidin-2(1H)-one (4b)

Yield: 2.65 g (73 %), White solid, mp. 136 °C. IR (KBr) (υ cm^{-1}): 1622 (C=O str.), 3093 (-CH- str.), 3214 (NH str.). ^{1}H NMR (DMSO-

d_6, 400 MHz) δ in ppm = 2.64 (s, 3H), 6.13 (s, 1H), 6.82 (s, 1H), 7.43 (m, 3H), 7.49 (m, 3H), 7.85 (m, 5H, Ar), 10.14 (s, 2H). ^{13}C NMR (100 MHz, DMSO-d_6) δ in ppm: 17.5 (*C*H$_3$), 39.49 (ring-*C*H), 98.9, 114.9, 125.7, 124.8, 132.2, 139.8, 148.8, 150.4 (ring *C*=O), 162.1, 167.2 (Thiazole C_2). Mass (*m/z*): 348.

3.5.3. 5-(5-([4-bromophenyl]amino)thiazol-2-yl)-4-(3-chlorophenyl)-6-methyl-3,4-dihydropyrimidin-2(1H)-one (4c)

Yield: 3.57 g (75 %), pale yellow solid, mp. 165 °C. IR (KBr) (υ cm^{-1}): 1675 (C=O str.), 3027 (-CH- str.), 3224 (NH str.). ^{1}H NMR (DMSO-d_6, 400 MHz) δ in ppm = 2.98 (s, 3H), 6.03 (s, 1H), 6.86 (s, 1H), 7.61 (d, 2H, J = 8.6 Hz), 7.72 (d, 2H, J = 8.4 Hz), 8.32 (m, 4H, Ar), 10.2 (s, 2H, NH). ^{13}C NMR (100 MHz, DMSO-d_6) δ in ppm: 17.1 (*C*H$_3$), 33.8 (ring-*C*H), 106.5, 134.5, 135.5, 138.5, 142.0, 143.1, 144.2, 149.3, 153.4 (ring *C*=O), 168 (Thiazole C_2). Mass (*m/z*): 473 (M$^+$), 475 (M+2).

3.5.4. 4-(3-Chlorophenyl)-5-(5-([3-chlorophenyl]amino)thiazol-2-yl)-6-methyl-3,4-dihydropyrimidin-2(1H)-one (4d)

Yield: 3.24 g (75 %), yellow solid, mp. 164 °C. IR (KBr) (υ cm^{-1}): 1676 (C=O str.), 3027 (-CH- str.), 3230 (NH str.). ^{1}H NMR (DMSO-d_6, 400 MHz) δ in ppm = 2.56 (s, 3H), 6.10 (s, 1H), 6.85 (m, 4H), 7.02 (m, 2H), 7.08 (m, 2H), 7.20 (m, 2H), 9.47 (s, 2H, NH). ^{13}C NMR (100 MHz, DMSO-d_6) δ in ppm: 17.2 (*C*H$_3$), 39.6 (ring-*C*H), 121.0, 132.9, 136.2, 138.6, 144.1, 154.7 (ring *C*=O), 168.6, 170.9 (Thiazole C_5). Mass (*m/z*): 431 (M$^+$), 433 (M+2).

3.5.5. 4-(3-Chlorophenyl)-5-(5-([4-chlorophenyl]amino)thiazol-2-yl)-6-methyl-3,4-dihydropyrimidin-2(1H)-one (4e)

Yield: 3.1 g (72 %), pale yellow solid, mp. 166 °C. IR (KBr) (υ cm^{-1}): 1652 (C=O str.), 3093 (-CH- str.), 3233 (NH str.). ^{1}H NMR (DMSO-d_6, 400 MHz) δ in ppm = 3.02 (s, 3H), 6.12 (s, 1H), 7.25 (m, 2H), 7.34 (m, 2H), 7.51 (m, 6H, Ar), 10.232 (s, 2H, NH). ^{13}C NMR (100 MHz, DMSO-d_6) δ in ppm: 17.4 (*C*H$_3$), 39.9 (ring-*C*H), 122.1, 132.9, 136.3, 138.5, 144.2, 154.7 (ring *C*=O), 168.5, 170.8 (Thiazole C_2). Mass (*m/z*): 430 (M$^+$), 432 (M+2).

3.5.6. 5-(5-([4-Bromophenyl] amino) thiazol-2-yl)-6-methyl-4-phenyl-3,4-dihydropyrimidin-2(1H)-one (4f)

Yield: 3.1 g (70 %), pale brown solid, mp. 170 °C. IR (KBr) (υ cm^{-1}): 1624 (C=O str.), 3089 (-CH- str.), 3234 (NH str.). ^{1}H NMR (DMSO-d_6, 400 MHz) δ in ppm = 2.64 (s, 3H), 6.10 (s, 1H), 7.45 (m, 4H), 7.50 (d, 2H, J = 8.6 Hz), 7.85 (m, 5H, Ar), 10.13 (s, 2H). ^{13}C NMR (100 MHz, DMSO-d_6) δ in ppm: 17.0 (*C*H$_3$), 33.8 (ring-*C*H), 134.3, 135.4, 138.5, 138.6, 142.0, 142.1, 143.1, 143.3, 144.2, 149.3, 151.3 (ring *C*=O), 169.4 (Thiazole C_2). Mass (*m/z*): 440 (M$^+$), 441 (M+1).

3.5.7. 5-(5-([4-Chlorophenyl]amino)thiazol-2-yl)-6-methyl-4-phenyl-3,4-dihydropyrimidin-2(1H)-one (4g)

Yield: 2.98 g (75 %), yellow crystals, mp. 169 °C. IR (KBr) (υ cm^{-1}): 1653 (C=O str.), 3093 (-CH- str.), 3230 (NH str.). ^{1}H NMR (DMSO-d_6, 400 MHz) δ in ppm = 2.64 (s, 3H), 6.22 (s, 1H), 7.45 (m, 4H), 7.49 (m, 2H), 7.85 (m, 5H, Ar), 10.13 (s, 2H). ^{13}C NMR (100 MHz, DMSO-d_6) δ in ppm: 17.3 (*C*H$_3$), 33.9 (ring-*C*H), 134.3, 135.4, 138.5, 138.6, 142.0, 143.2, 144.2, 149.2, 151.3, 153.3 (ring *C*=O), 170.0 (Thiazole C_2). Mass (*m/z*): 396 (M$^+$), 398 (M+2).

3.5.8. 5-(5-([3-Chlorophenyl]amino)thiazol-2-yl)-6-methyl-4-phenyl-3,4-dihydropyrimidin-2(1H)-one (4h)

Yield: 3.02 g (76 %), yellow crystals, mp. 170 °C. IR (KBr) (υ cm^{-1}): 1644 (C=O str.), 3088 (-CH- str.), 3226 (NH str.). ^{1}H NMR (DMSO-d_6, 400 MHz) δ in ppm = 2.64 (s, 3H), 6.16 (s, 1H), 7.44 (m, 4H), 7.50 (d, 2H, J = 8.6 Hz), 7.85 (m, 5H, Ar), 10.13 (s, 2H). ^{13}C NMR (100 MHz, DMSO-d_6) δ in ppm: 17.2 (*C*H$_3$), 33.8 (ring-*C*H), 134.3, 135.4, 138.5, 138.6, 142.0, 142.1, 143.1, 144.1, 149.2, 151.3 (ring *C*=O), 169.1 (Thiazole C_2). Mass (*m/z*): 430 (M$^+$), 432 (M+2).

3.6. Biological activities

3.6.1. Antibacterial activity

The study utilized a clinical strain of *Bacillus cereus* (*B. cereus*), *Staphylococcus aureus* (*S. aureus* ATCC 6538), and *Listeria monocytogenes* (*L. monocytogenes*) for the experiment. While *Escherichia coli* (*E. coli* ATCC 35210), *Enterobacter cloacae* (*E. cloacae* clinical isolate), and various other strains belonged to the Gram-negative bacteria group, *Salmonella typhimurium* (*S. Typhimurium* ATCC 13311) was classified as a Gram-positive bacterium. Resistant strains such as *S. aureus*, *E. coli*, and various isolates of *Pseudomonas aeruginosa* (*P. aeruginosa*) were also included in the study. The isolates were obtained using Kartsev et al.'s approach [38].

3.6.2. In vitro anti-inflammatory activity (denaturation of bovine serum albumin method)

The anti-inflammatory activity of the target compounds was measured using the denaturation of bovine serum albumin technique, in accordance with the methods outlined in the literature [39,40]. In the test sample, the pH of the combination, which contained the test chemical and a 1 % aqueous solution of bovine albumin fraction was increased to 7.4. Furthermore, test samples were incubated for 20 min at 37 °C before being heated to 51 °C for 20 min. A UV–visible spectrophotometer was used to measure the turbidity of the sample at 660 nm after it had cooled to room temperature. Diclofenac sodium, the characteristic medicine used in the investigation, was administered in triplicate. Based on the percentage of inhibition of albumin denaturation, the following calculation was used to calculate the anti-inflammatory activity of the titled compounds as given below.

$$\%\ of\ Inhibition = \frac{[Controlled\ optical\ density(OD) - Sample\ OD]}{Controlle\ OD} \times 100$$

3.6.3. Antioxidant activity in terms of DPPH radical inhibition assay

The ability of hydrazone analogs to scavenge free radicals was examined using the previous literature [41]. At various doses (20–100 μg/mL), a recently prepared DPPH solution (0.004 % w/v) was added to the sample solutions in methanol. The solution was allowed to be placed at room temperature for 30 min in the dark. Next, using a spectrometer, the mixture's absorbance, or optical density) at 517 nm was measured. Ascorbic acid was the drug used as a reference. Methanol served as the blank, and the same volume of DPPH was used to create the control sample in the absence of any test samples. The lower absorbance value of the reaction mixture indicates that it has a higher free radical scavenging activity. Every test was administered three times in duplicate. Using the following formula, the fraction of the DPPH free radical that was scavenged was calculated:

$$\%\ \text{Inhibition} = \frac{(A_{control} - A_{test})}{A_{control}} \times 100$$

where, $A_{control}$ represents the absorbance of the control reaction and A_{test} is the test sample absorbance.

3.7. Corrosion inhibition studies

3.7.1. Preparation of specimen and electrolyte preparation

In the experiment, a mild steel (MS) substrate with an actual size of 1 cm^2 was utilized as the working electrode. The specimens were embedded in epoxy resin, leaving a designated working area. To prepare the surface of the specimens, different grades (100, 400, 800, and 1200) of emery paper were employed. Subsequently, the specimens were cleaned with acetone, rinsed with distilled water, dried, and promptly used for analysis. For the corrosive medium, a 1 M HCl solution was prepared by diluting 37 % HCl (Merck) with distilled water. This solution served as the electrolyte. To investigate the inhibition effect, inhibitor solutions were prepared by dissolving 100 mg/L of the inhibitor in the 1 M HCl acid solution.

3.7.2. Corrosion analysis

A potentiostat (CH604 E-series, U.S. type) outfitted with CH-instrument beta software was used for the electrochemical investigations. A glass cell with three electrodes was used for two different kinds of measurements, PP, and EIS. A polished MS specimen was used as the working electrode, and platinum and calomel electrodes were used as the counter and reference electrodes respectively. For the studies, 1 M HCl was used as a corrosive medium and was conducted at room temperature (30 °C). An open circuit potential (OCP) was allowed to stabilize the MS specimen, which had an exposed area of 1 cm^2. The next step involved conducting PP investigations by scanning within a potential range of ±200 mV at a scan rate of 0.001 mVs^{-1} from the OCP. The Tafel (I-E) plots that resulted were then recorded, making it possible to calculate the corrosion rates, corrosion potential, and corrosion current density (E_{corr}, I_{corr}). To assess the efficacy of inhibitors, tests were conducted in both their presence and absence. Based on the observed corrosion rates, the percentage inhibition efficiency (% IE) was computed. Potentiodynamic polarization was combined with research using electrochemical impedance spectroscopy (EIS). At the OCP, an AC signal with an amplitude of 10 mV was applied, with a frequency range spanning from 100 kHz to 10 mHz [41].

3.8. DFT studies

Understanding the energy difference between the highest occupied (HOMO) and lowest unoccupied (LUMO) molecular orbitals is crucial for analyzing the absorption of electronic transitions in molecular systems. This energy difference directly influences the excitation energy of a molecule. Understanding the molecular orbitals gives us valuable information about the reactivity, physical characteristics, and structure of molecules. The figures illustrate the positive and negative phases using red and green colors, respectively. By employing the B3LYP/6-31G (d,p) technique, the computed HOMO-LUMO energies and energy gap for the compounds being studied are determined [42].

3.9. Molecular docking studies

3.9.1. Protein preparation

The protein database (www.rcsb.org) provided the crystal structures of celecoxib bound at the COX-2 active site (PDB: 3LN1) [43]. The inhibitors, additional ligands, and water molecules were removed from the protein before protein production to obtain clean protein. Before docking, the protein was supplemented with polar hydrogen atoms bearing Gasteiger-Huckel charges [44]. There were 62, 66, and 38 points in the centre of the protein (PDB ID: 3LN1) grid box, and 37.738, −26.122, and −6.412 Å were the number of points in the x, y, and z dimensions, respectively.

3.9.2. Ligand preparation

The produced molecules were orientated in two dimensions using the Marvin Sketch tool. A minimization technique was then employed to transform the two-dimensional structures into the three-dimensional ones that would require the least amount of energy. Additionally, the assertions made by Gasteiger Using Auto Dock 4.2, rotatable bonds and nonpolar hydrogen atoms were created. Auto Dock Vina was used to dock each molecule. The docking result is shown by the software Discovery Studio [45].

4. Conclusions

For this study, a range of novel thiazole derivatives was synthesized and determined their effectiveness against different bacterial and fungal pathogens, specifically in terms of their antibacterial and antifungal properties. The compounds that were tested, showed a range of antibacterial activity, with MIC values ranging from 0.23 to >3.75 mg/mL and MBC values ranging from 0.35 to >3.75 mg/mL. Out of all the compounds that were tested, **4d** and **4h** displayed the most potent activity against *E. coli*, *B. cereus*, and *S. typhimurium*, respectively, with MIC/MBC values of 0.17/0.23 mg/mL. In addition, three highly active compounds (**4b**, **4c**, and **4d**) were tested against three strains that have shown resistance: MRSA, *E. coli*, and *P. aeruginosa*. These compounds showed superior activity in comparison to the reference drugs against MRSA, and compound **4d** also displayed activity against *P. aeruginosa*. Thiazoles were screened for anti-inflammatory activity among the synthesized compounds, **4a** and **4c** possess excellent anti-inflammatory potency. Thiazoles were screened for antioxidant activity and **4a** and **4c** stood highly potent for antioxidant study. In addition, compound **4c** demonstrated excellent inhibition efficiency on mild steel in a 1 N HCl solution, as verified through PP and EIS techniques. The inhibitory effectiveness of pyrimidine-substituted thiazole derivatives was further supported by DFT calculations. This work focuses on the synthesis and evaluation of thiazole derivatives that show great potential as antibacterial and antifungal agents. Additionally, these derivatives have been studied for their ability to inhibit corrosion, with supporting evidence from DFT calculations. Further *in silico* studies of the synthesized thiazoles confirmed the good interactions with the target. With the in-depth structure-activity relationship, synthesis of a library of compounds with further derivation of pyrimidinone linked thiazoles and pyrimidinone linked quinoxalines are in progress in our laboratory and the results will be published as a separate article in future.

CRediT authorship contribution statement

K.D. Venu prasad: Writing – original draft, Visualization, Software, Methodology. **Balakrishna Kallauraya:** Writing – review & editing, Supervision. **Ramesh S. Bhat:** Writing – review & editing, Supervision, Project administration, Investigation, Conceptualization. **Subrahmanya I. Bhat:** Visualization, Validation, Formal analysis, Data curation, Conceptualization. **Vinuta Kamat:** Visualization, Software, Resources, Methodology, Conceptualization. **Mahesh Akki:** Writing – original draft, Validation, Software, Formal analysis, Data curation. **Amit Kumar:** Visualization, Validation, Project administration, Investigation, Conceptualization. **K. Jyothi:** Software, Formal analysis, Conceptualization. **B.R. Bharat:** Visualization, Validation, Investigation, Formal analysis, Conceptualization.

Declaration of competing interest

The authors declare the following financial interests/personal relationships which may be considered as potential competing interests:Dr. Subrahmanya I Bhat is working as an Associate editor for Heliyon, Chemistry and followed the journal ethics and publishing policies.

References

[1] H.S. Gold, R.C. Moellering Jr., Antimicrobial-drug resistance, New England J.med. 335 (19) (1996) 1445–1453.
[2] K. Nepali, S. Sharma, M. Sharma, P. Bedi, K. Dhar, Rational approaches, design strategies, structure activity relationship and mechanistic insights for anticancer hybrids, Eur. J. Med. Chem. 77 (2014) 422–487.
[3] M.H. Cohen, J.R. Johnson, R. Justice, R. Pazdur, FDA drug approval summary: nelarabine (Arranon®) for the treatment of T-cell lymphoblastic leukemia/lymphoma, Oncol. 13 (6) (2008) 709–714.
[4] O.I. El-Sabbagh, M.M. Baraka, S.M. Ibrahim, C. Pannecouque, G. Andrei, R. Snoeck, J. Balzarini, A.A. Rashad, Synthesis and antiviral activity of new pyrazole and thiazole derivatives, Eur. J. Med. Chem. 44 (9) (2009) 3746–3753.
[5] K.-M. Cheng, Y.-Y. Huang, J.-J. Huang, K. Kaneko, M. Kimura, H. Takayama, S.-H. Juang, F.F. Wong, Synthesis and antiproliferative evaluation of N, N-disubstituted-N′-[1-aryl-1H-pyrazol-5-yl]-methnimidamides, Bioorg. Med. Chem. Lett. 20 (22) (2010) 6781–6784.
[6] H.M. Faidallah, M.M. Al-Mohammadi, K.A. Alamry, K.A. Khan, Synthesis and biological evaluation of fluoropyrazolesulfonylurea and thiourea derivatives as possible antidiabetic agents, J. Enzym. Inhib. Med. Chem. 31 (sup1) (2016) 157–163.
[7] Y. Al-Humaidi Jehan, Sobhi M. Gomha, Nahed A. Abd El-Ghany, Basant Farag, Magdi E.A. Zaki, Tariq Z. Abolibda, Nadia A. Mohamed, Using terephthalohydrazide chitosan hydrogel as ecofriendly biopolymeric catalyst, Catalysts 13 (9) (2023) 1311.
[8] Mosaad Abdallah Abanoub, Sobhi M. Gomha, Magdi E.A. Zaki, Tariq Abolibda, Nabila A. Kheder, A Green Synthesis, DFT calculations, and molecular docking study of some new indeno[2,1-b]quinoxalines containing thiazole moiety, J. Mol. Struct. 1292 (2023) 136044, https://doi.org/10.1016/j.molstruc.2023.136044.
[9] V. Kamat, R. Santosh, B. Poojary, S.P. Nayak, B.K. Kumar, M. Sankaranarayanan, Faheem, S. Khanapure, D.A. Barretto, S.K. Vootla, Pyridine-and thiazole-based hydrazides with promising anti-inflammatory and antimicrobial activities along with their in-silico studies, ACS Omega 5 (39) (2020) 25228–25239.
[10] X. Zhu, Y. Zhang, Z. Ma, Y. He, P. Song, R. Wang, Construction of thiazole-zwitterionic copolymer nanospheres with iso-bifunctional groups for excellent antibacterial activity, Prog. Org. Coating 186 (2024) 108084.
[11] P.N. Gopal, S. Poda, B.S. Swetha, S. Gadde, Synthesis, charectertisation and antitubercular evaluation of pyarzoline clubbed thiazole hybrids, Curr. Trends Biotechnol. Pharm. 18 (2) (2024) 1788–1797.
[12] B. Kallauraya, K. Venuprasad, R.S. Bhat, A. D'Souza, P. Nayak, R. Gururaja, Synthesis of Novel [2-(2-(4-Halo Substituted Phenyl), Quinoline-4-Carbonyl)-5-Methyl-4-(2-Phenylhydrazineylidene)-2, 4-dihydro-3h-pyrazol-3-one] hybrids and its pharmacological studies, Rasayan J. Chem. 16 (2) (2023).
[13] K. Girisha, B. Kalluraya, J.H. Vidyashree, Synthesis, characterisation, and antimicrobial activity of 3-methyl-6-(aryl)-1-phenyl-1H-pyrazolo [3, 4-b] pyridine, Indian J. Chem. 44 (15) (2012) 1767–1770.
[14] Jehan Y. Al-Humaidi, Sobhi M. Gomha, Sayed M. Riyadh, Mohamed S. Ibrahim, Magdi E.A. Zaki, Tariq Z. Abolibda, Ohoud A. Jefri, Amr S. Abouzied, Synthesis, biological evaluation, and molecular docking of novel azolylhydrazonothiazoles as potential anticancer agents, ACS Omega 8 (37) (2023) 34044–34058.
[15] Maher Abd El-Aziz El-Hashash, Sobhi Mohamed Gomha, Elham Ezz El-Arab, Utility of pyrazolylchalcone synthon to synthesize azolopyrimidines under grindstone technology, Chem. Pharm. Bull. (Tokyo) 65 (1) (2017) 90–96.

[16] S.A. Rostom, I.M. El-Ashmawy, H.A. Abd El Razik, M.H. Badr, H.M. Ashour, Design and synthesis of some thiazolyl and thiadiazolyl derivatives of antipyrine as potential non-acidic anti-inflammatory, analgesic and antimicrobial agents, Bioorg. Med. Chem. 17 (2) (2009) 882–895.
[17] S. Bondock, W. Fadaly, M.A. Metwally, Synthesis, and antimicrobial activity of some new thiazole, thiophene and pyrazole derivatives containing benzothiazole moiety, Eur. J. Med. Chem. 45 (9) (2010) 3692–3701.
[18] D. Havrylyuk, O. Roman, R. Lesyk, Synthetic approaches, structure activity relationship and biological applications for pharmacologically attractive pyrazole/pyrazoline–thiazolidine-based hybrids, Eur. J. Med. Chem. 113 (2016) 145–166.
[19] G. Kumari, S. Dhillon, P. Rani, M. Chahal, D.K. Aneja, M. Kinger, Development in the synthesis of bioactive thiazole-based heterocyclic hybrids utilizing phenacyl bromide, ACS Omega 9 (17) (2024) 18709–18746.
[20] Ankit Kumar, Efthalia Angelopoulou, Efstratios-Stylianos Pyrgelis, Christina Piperi, Awanish Mishra, Harnessing therapeutic potentials of biochanin A in neurological disorders: pharmacokinetic and pharmacodynamic overview, Chem. Biodiversity 21 (8) (2024) e202400701.
[21] Abdou O. Abdelhamid, Sobhi M. Gomha, Waleed A.M. A. El-Enany, Efficient synthesis and antimicrobial evaluation of new azolopyrimidines-bearing pyrazole moiety, J. Heterocycl. Chem. 56 (2019) 2487–2493.
[22] Mohammad Qneibi, Mohammed Hawash, Mehmet Gümüş, Irfan Capan, Yusuf Sert, Sosana Bdir, İrfan Koca, Mohammad Bdair, Deciphering the biophysical properties of ion channel gating pores by coumarin-benzodiazepine hybrid derivatives: selective AMPA receptor antagonists, Mol. Neurobiol. 61 (2024) 4565–4576.
[23] Necmi Dege, Halil Gökce, Onur Erman Doğan, Gökhan Alpaslan, Tuğgan Ağar, Sobanraj Muthu, Yusuf Ser, Quantum computational, Spectroscopic investigations on N-(2-((2-chloro-4,5-dicyanophenyl)amino)ethyl)-4-methylbenzenesulfonamide by DFT/TD-DFT with different solvents, molecular docking and drug-likeness researches, Coll. Surf. A Physicochem. and Eng. Aspects 638 (2022) 128311.
[24] Ibadulla Mahmudov, Yeliz Demir, Yusuf Sert, Yusif Abdullayev, Afsun Sujayev, Saleh Alwasel, Ilhami Gülçin, Synthesis and inhibition profiles of N-benzyl-and N-allyl aniline derivatives against carbonic anhydrase and acetylcholinesterase-A molecular docking study. Arab. J. Chem., 15(4):103645, DOI:10.1016/j.arabjc.2021.103645.
[25] Irfan Çapan, Mohammed Hawash, Mohammed T. Qaoud, Levent Gülüm, Ezgi Nurdan Yenilmez Tunoglu, Kezban Ucar Cifci, Bekir Sıtkı Çevrimli, Yusuf Sert, Süleyman Servi, İrfan Koca, Yusuf Tutar, BMC chem 18 (1) (2024) 102.
[26] P. Biginelli, Aldehyde-urea derivatives of aceto- and oxaloacetic acids. Gazz. Chim. Ital. 23 (1893) 360–413.
[27] R. Kaur, S. Chaudhary, K. Kumar, M.K. Gupta, R.K. Rawal, Recent synthetic and medicinal perspectives of dihydropyrimidinones: a review, Eur. J. Med. Chem. 132 (2017) 108–134.
[28] S. Bijani, F. Shaikh, S. Mirza, S.W.I. Siu, N. Jain, R. Rawal, N.G.J. Richards, A. Shah, A. Radadiya, Novel dihydropyrimidinone derivatives as potential P-glycoprotein modulators, ACS Omega 7 (19) (2022) 16278–16287.
[29] K. Ul Haq, N.L. Saadah, I. Siswanto, H. Suwito, Bioactivity of dihydropyrimidinone derivatives as inhibitors of cyclooxygenase-2 (COX-2): an in-silico approach, RSC Adv. 13 (2023) 34348–34357.
[30] N.S. Naik, L.A. Shastri, S.D. Joshi, S.R. Dixit, B.M. Chougala, S. Samundeeswari, M. Holiyachi, F. Shaikh, J. Madar, R. Kulkarni, V. Sunagar, 3,4-Dihydropyrimidinone-coumarin analogues as a new class of selective agent against *S. aureus*: synthesis, biological evaluation, and molecular modelling study, Bioorg. Med. Chem. 25 (4) (2017) 1413–1422.
[31] Dihydropyrimidinones and -thiones with improved activity against human polyomavirus family members Alexandra Manos-Turvey Hiba A. Al-Ashtal, Patrick G. Needham, Caroll B. Hartline, Mark N. Prichard, Peter Wipf, Jeffrey L. Brodsky, Bioorg. Med. Chem. Lett. 26 (20) (2016) 5087–5091.
[32] Zhang Zhang, Shi-Hong Lu, Bin Xu, Xi-Cun Wang, A domino desulfitative coupling and decarboxylative coupling of 3,4-dihydropyrimidine-2-thiones with copper(I) carboxylates, Bioorg. Chem. 28 (5) (2017) 1074–1078.
[33] K. Raviprabha, R.S. Bhat, Inhibition effects of ethyl-2-amino-4-methyl-1, 3-thiazole-5-carboxylate on the corrosion of AA6061 alloy in hydrochloric acid media, J. Fail. Anal. Prev. 19 (5) (2019) 1464–1474.
[34] S.B. Rose, R.E. Miller, Studies with the agar cup-plate method: I. A standardized agar cup-plate technique, J. Bacteriol. 38 (5) (1939) 525–537.
[35] Y. Mizushima, M. Kobayashi, Interaction of anti-inflammatory drugs with serum proteins, especially with some biologically active proteins, J. Pharm. Pharmacol. 20 (3) (1968) 169–173.
[36] Hanane Kaoukabi, Youssef Kabri, Christophe Curti, Moha Taourirte, Juan C. Rodriguez-Ubis, Robert Snoeck, Graciela Andrei, Patrice Vanelle, B. Hassan, Lazrek, Dihydropyrimidinone/1,2,3-triazole hybrid molecules: synthesis and anti-varicella-zoster virus (VZV) evaluation, Eur. J. Med. Chem. 155 (2018) 772–781.
[37] W.M. Haynes (Ed.), CRC Handbook of Chemistry and Physics, 94th Edition, CRC Press LLC, Boca Raton, 2013-2014, pp. 343–458. FL.
[38] S. Sakat, P. Tupe, A. Juvekar, Gastroprotective effect of methanol extract of Oxalis corniculata Linn (whole plant) experimental animals, Planta Med. 76 (12) (2010) P090.
[39] R. Santosh, M.K. Selvam, S.U. Kanekar, G.K. Nagaraja, Synthesis, characterization, antibacterial and antioxidant studies of some heterocyclic compounds from triazole-linked chalcone derivatives, Chem. Sel. 3 (23) (2018) 6338–6343.
[40] Y.N. Mabkhot, F.D. Aldawsari, S.S. Al-Showiman, A. Barakat, S.M. Soliman, M.I. Choudhary, S. Yousuf, M.S. Mubarak, T.B. Hadda, Novel enaminone derived from thieno [2, 3-b] thiene: synthesis, x-ray crystal structure, HOMO, LUMO, NBO analyses and biological activity, Chem. Cent. J. 9 (2015) 1–11.
[41] K. Raviprabha, R.S. Bhat, Corrosion inhibition effect of ethyl 1-(4-chlorophenyl)-5-methyl-1 H-1, 2, 3-triazole-4-carboxylate on aluminium alloy in hydrochloric acid, Protect. Met. Phys. Chem. Surface 57 (1) (2021) 181–189.
[42] P.R. D'Souza, J. Kudva, A.S. Kumar, A.N. Shetty, Experimental and computational studies of N-(4, 6-dimethylpyrimidin-2-yl)-4-[(quinazoline-4-yl) amino]-benzene-1-sulfonamide as an effectual corrosion inhibitor for mild steel in hydrochloric acid, Russ. J. Appl. Chem. 94 (2021) 1122–1133.
[43] J.L. Wang, D. Limburg, M.J. Graneto, J. Springer, J.R.B. Hamper, S. Liao, J.L. Pawlitz, R.G. Kurumbail, T. Maziasz, J.J. Talley, The novel benzopyran class of selective cyclooxygenase-2 inhibitors. Part 2: the second clinical candidate having a shorter and favorable human half-life, Bioorg. Med. Chem. Lett. 20 (23) (2010) 7159–7163.
[44] V. Babagond, K. Katagi, M. Akki, D.S. Reddy, H. Shanavaz, A. Jaggal, S. Dk, Design and synthesis of potent anticancer agents using coumarin-quinazolinone based scaffolds: exploration of ADME properties and molecular docking studies, Chem. Sel. 9 (17) (2024) e202400435.
[45] O. Trott, A.J. Olson, AutoDock Vina: improving the speed and accuracy of docking with a new scoring function, efficient optimization, and multithreading, J. Comput. Chem. 31 (2) (2010) 455–461.